Jin et al. Nanoscale Research Letters (2015) 10:95
DOI 10.1186/s11671-015-0790-x

Nanoscale Research Letters
a SpringerOpen Journal

NANO EXPRESS Open Access

Structure and photoluminescence of the TiO_2 films grown by atomic layer deposition using tetrakis-dimethylamino titanium and ozone

Chunyan Jin[1], Ben Liu[1], Zhongxiang Lei[2] and Jiaming Sun[1*]

Abstract

TiO_2 films were grown on silicon substrates by atomic layer deposition (ALD) using tetrakis-dimethylamino titanium and ozone. Amorphous TiO_2 film was deposited at a low substrate temperature of 165°C, and anatase TiO_2 film was grown at 250°C. The amorphous TiO_2 film crystallizes to anatase TiO_2 phase with annealing temperature ranged from 300°C to 1,100°C in N_2 atmosphere, while the anatase TiO_2 film transforms into rutile phase at a temperature of 1,000°C. Photoluminescence from anatase TiO_2 films contains a red band at 600 nm and a green band at around 515 nm. The red band exhibits a strong correlation with defects of the under-coordinated Ti^{3+} ions, and the green band shows a close relationship with the oxygen vacancies on (101) oriented anatase crystal surface. A blue shift of the photoluminescence spectra reveals that the defects of under-coordinated Ti^{3+} ions transform to surface oxygen vacancies in the anatase TiO_2 film annealing at temperature from 800°C to 900°C in N_2 atmosphere.

Keywords: Atomic layer deposition; Titanium dioxide; Photoluminescence; Crystal structure; Defects; XPS

PACS: 81.15.Gh; 72.20.Jv; 78.20.Ci

Background

TiO_2 has become a promising material in different applications for its large band gap [1], high refractive index [2,3], high dielectric constant [4,5], and highly active surface. In terms of photochemical properties, TiO_2 is used in decomposition of water into hydrogen and oxygen [6] and served as a photocatalyst in solar cells [7]. Degradation of organic molecules is another active research topic, such as purification of waste water [8], disinfection in public [9], self-cleaning coating [10], corrosion-protection [11], and actively suppressed impact on tumor cells of rats illuminated by near-UV [12-14]. In addition, TiO_2, as a semiconducting metal oxide, can be used as oxygen gas sensor to control the air/fuel mixture in car engines [15,16]. The high dielectric constant broadens the applications of TiO_2 in electronics, such as capacitor and memory device. In our daily life, titanium dioxide pigment is almost used in every kind of paint because of its high refractive index. Moreover, pure TiO_2 is non-toxic and easy-dispersive, and it can be used in food additive [17], in cosmetic products, as well as in pharmaceuticals [18].

Among extensive applications using physical and surface chemical properties of TiO_2, the defects and the surface states of TiO_2, which depend strongly on material preparation technologies, play an important role in its electrical, chemical, as well as optical properties. Therefore, selection of a well-controllable technology to engineer the defects in TiO_2 will be crucial for specific application. Almost all viable physical and chemical deposition technologies have been adopted to prepare TiO_2 thin films. Atomic layer deposition (ALD) has distinguished advantages over others for its precise thickness control, extremely conformal surface coating for nanostructures, large area uniformity, and low growth temperature [19-21]. Several precursors have been applied successfully for deposition of TiO_2 by ALD processes. The common precursor, $TiCl_4$, is a liquid with a moderate vapor pressure [22-27]. In the ALD process with H_2O/H_2O_2 as oxidant, the corrosive by-products of HCl and residual $TiCl_4$ are considered as a drawback. Same as Ti halide, TiI_4 can also be served as another precursor [28-30] with relative less corrosive, compared

* Correspondence: jmsun@nankai.edu.cn
[1]Key Laboratory of Weak Light Nonlinear Photonics, Ministry of Education, School of Physics, Nankai University, Weijin Road 94, Tianjin 300071, China
Full list of author information is available at the end of the article

to $TiCl_4$. Recently, titanium alkoxides become promising precursors without corrosive halogen by-products, and research has been carried out on isopropoxide ($Ti(O^iPr)_4$) and titanium ethoxide ($Ti(OEt)_4$). Although high purity thin films can be grown at 300°C, the decomposition of precursor leads to an undistinguished ALD temperature window. In addition, titanium isopropoxide can be adopted as precursor in theory, but significant decomposition occurs at lower deposition temperature than that of the titanium ethoxide. Since the bond energy of metal-halide is much stronger than that of the metal-nitrogen bond, metal amide compounds are expected to have much higher reactivity with H_2O, and therefore, tetrakis-(dimethylamino) titanium (TDMAT) and H_2O have been used for ALD processes [31,32]. However, using H_2O as oxidant has two main disadvantages: the water vapor exposure on TiO_2 surface requires a very long purge time at the deposition temperature below 150°C [33], and the H_2O-based ALD process brings impurities, such as hydroxyl groups (–OH) in the films [34,35]. The "dry" ALD process of TiO_2 films using TDMAT and ozone (O_3) may have more advantages, comparing to the TDMAT and H_2O process. Only a few reports have been published concerning the TDMAT and O_3 process [36,37], and the study on controlling the transformation of structure and defects has not yet been done in ALD TiO_2 films. A comprehensive research on the thermal stability of the structure and defects in the ALD TiO_2 film is crucial for controlling its electric and optical properties for different applications.

In this study, TiO_2 films were deposited on silicon substrates by ALD technology using TDMAT and ozone process. The dependences of the growth rate, refractive index, and crystal structure and defects of the TiO_2 films on the growth temperatures are investigated in details by optical ellipsometry, X-ray diffraction (XRD), photoluminescence (PL), and X-ray photoelectron spectroscopy (XPS). Annealing processes were performed comparably on two as-grown TiO_2 films with amorphous and anatase phase structures, respectively. Thermal stability of the structure and defects in the as-grown TiO_2 films and those annealed at different temperatures were studied by PL spectroscopy in conjunction with XRD and XPS analysis. Amorphous, anatase, and rutile TiO_2 films were prepared at different ALD growth temperatures or by annealing at different temperatures. The PL spectra show a red band at 600 nm and a green band at around 515 nm from the defects in anatase TiO_2 films. It was shown that the red band has a strong correlation with the defects associated with under-coordinated Ti^{3+} ions and the green band is related to the oxygen vacancies on (101) surface of anatase TiO_2 films. The blue shift of the PL spectra indicates that the defects in anatase TiO_2 film undergo a transformation from under-coordinated Ti atoms to surface oxygen vacancies with increasing the annealing temperature from 800°C to 900°C in N_2 atmosphere.

Methods

TiO_2 films were deposited on 4-in. (100) oriented n-type silicon wafers by a small chamber ALD system (Cambridge NanoTech Savannah 100, Cambridge NanoTech Inc., Cambridge, MA, USA) using TDMAT and O_3. The evaporation temperature of the TDMAT source was kept at 60°C, and the precursor delivery lines were heated at 150°C. O_3 was generated from high purity O_2 (99.999%) through an ozone generator with an O_2/O_3 flow of 500 sccm and O_3 concentration of 36 mg/L. High purity nitrogen gas (99.999%) was used as a carrying and purging gas with a flow rate of 20 sccm. Before the film deposition, the Si wafer was cleaned through the standard process of Radio Corporation of America (RCA), followed by a final cleaning in diluted HF solution. TiO_2 samples with 1,000 ALD cycles were deposited at different substrate temperatures varying from 75°C to 400°C. One TiO_2 deposition cycle consists of 0.5 s TDMAT pulse time, 5 s N_2 purge, 1.8 s O_2/O_3 pulse time, and 9 s N_2 purge, respectively. The thermal stability of the structures of ALD TiO_2 films was studied by annealing two as-grown ALD samples with different initial structures; one is an amorphous TiO_2 film grown at low substrate temperature of 165°C, and the other is an anatase TiO_2 film grown at 250°C. The annealing treatment was taken at different temperatures from 250°C to 1,150°C in a flowing N_2 atmosphere for 1 h.

The crystallinity of the TiO_2 films was characterized by XRD with Cu K_α radiation. The thickness and refractive index of the TiO_2 films on Si substrates were measured by an ellipsometer with a 632.8-nm He-Ne laser beam at an incident angle of 69.8°. The film growth per cycle was calculated by dividing the film thickness with the total number of ALD cycles. PL spectra of the TiO_2 films were measured at room temperature under the excitation of the 266-nm line of a pulsed diode pumped Q-switch solid state laser (CryLas DX-Q, CryLaS GmbH, Berlin, Germany). The PL signal was collected by a 1/2 meter monochromator and detected by a photomultiplier (model H7732-10, Hamamatsu Corporation, Shimokanzo, Iwata, Japan) connected to a computer-controlled Keithley 2010 multimeter (Keithley Instruments Inc., Cleveland, OH, USA). XPS measurement was performed in a Kratos Axis Ultra DLD spectrometer (Kratos Analytical Ltd, Britain). Monochromatized Al-Kα X-ray source (h_γ = 1,486.6 eV) was utilized to excite TiO_2 thin films. X-ray photoelectron spectra were measured from the surface of the TiO_2 samples annealed at 350°C, 600°C, 800°C, 850°C, and 1,000°C. For comparison, XPS was measured from the sample annealed at 1,000°C after removing 3 nm of the surface layer by Ar^+ ion sputtering. The Ar^+ ion sputtering was performed over an area of 2 × 2 mm^2, using an ion current

of about 100 mA. The binding energy of each spectrum was calibrated by using the standard energy of carbon C1s peak at 284.6 eV.

Results and discussion

Figure 1 shows the dependences of the growth per cycle and the refractive index of the TiO_2 films on the growth temperature. Initially, the growth rate of the TiO_2 films decreases from 0.52 to 0.45 Å/cycle with increasing temperature from 75°C to 100°C, then a saturated growth window appears at the growth temperature from 100°C to 250°C, with a stable self-limiting growth rate of 0.46 Å/cycle. Further increasing the growth temperature above 300°C, the growth rate strongly increases. The growth rate in Figure 1 is consistent with the results in ref. [37] in the same temperature range, which showed an ALD temperature window of 150°C to 225°C and a deposition rate of 0.44 ± 0.15 Å/cycle, respectively.

The dependence of the growth per cycle on the growth temperature in this O_3-based process is different from that of the TDMA and H_2O process reported in ref. [31,32,38]. In the H_2O-based process, where -OH groups are the reactive sites, the deposition rate decreases with increasing the growth temperature from 80°C to 350°C. The growth rate of TiO_2 at growth temperature below 150°C could be strongly influenced by the purging time of H_2O vapor. The reported results on the growth rate per cycle are controversial using TDMAT and H_2O process, depending on the ALD systems used by different groups. Lim and Kim observed a narrow ALD window between 120°C and 150°C in the TDMAT and H_2O process [31], whereas other reports showed a decrease of the growth rate with increasing temperature from 150°C up to 350°C, without distinguished saturated growth temperature window [32,39]. This is probably due to the insufficient evacuation of the residual H_2O vapor in the growth chamber [40]. The decrease of the growth rate in the H_2O-based process with increasing the growth temperature was probably caused by the strong thermal desorption of the intermediate product mediated by -OH group adsorption on the surface, as proposed in ref. [32]. The possible chemical reaction of the surface species with -OH groups is:

$$\mathrm{TiO_2\text{-}O\text{-}Ti}\left[\mathrm{N(CH_3)_2}\right]_3{}^{*} + \mathrm{TiO_2\text{-}OH^{*}} \rightarrow \mathrm{TiO_2\text{-}O^{*}\text{-}TiO_2} + \mathrm{HOTi}\left[\mathrm{N(CH_3)_2}\right]_3\uparrow.$$

On the contrary, in the O_3-based process, the desorption of intermediate products is suppressed without the surface adsorption of the -OH groups from H_2O vapor; therefore, a wider ALD saturated growth temperature window from 100°C to 250°C was observed, and the growth rate shows a strong increase of from 0.58 to 4.08 Å/cycle with increasing the growth temperature from 250°C to 400°C. The strong increase of the growth rate is due to the chemical vapor deposition (CVD) process which is related to the strong thermal decomposition of the TDMAT precursor [41,42] at temperature above 250°C.

Figure 2 shows the XRD patterns of the TiO_2 films deposited at different growth temperatures from 175°C to 400°C. Initially, the films deposited at temperatures below 175°C are amorphous. With increasing growth temperature from 200°C to 250°C, the films show anatase crystal phase, with the (101) and (200) peaks in the diffraction patterns. The intensity of the anatase (101) peak reaches a maximum at the growth temperature of 250°C and then decreases dramatically to 300°C, with an emergence of a weak (110) peak from rutile TiO_2. At growth temperature above 250°C, the growth mode of the films changes to fast CVD mode, the fast deposition rate causes a strong degradation of the crystallinity of the TiO_2 film, as shown by the decrease of the diffraction peaks in the XRD patterns at 300°C to 400°C. Despite of this, very weak (101) peak from anatase TiO_2 and (110) peak from rutile

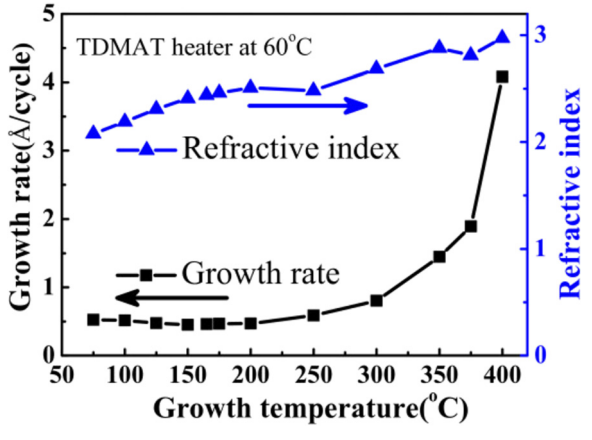

Figure 1 Dependences of the growth per cycle and refractive index on the growth temperature. The TiO_2 films were deposited on Si (100) substrates with 1,000 ALD cycles.

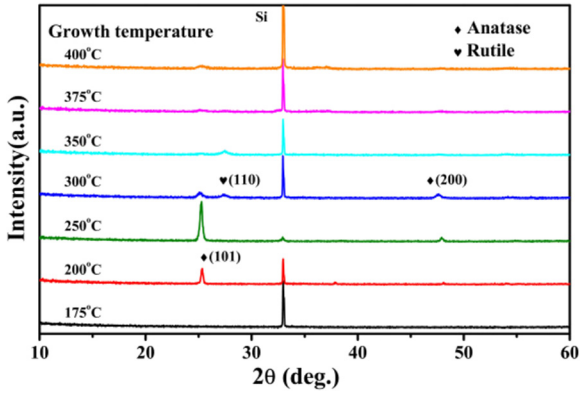

Figure 2 XRD patterns of the TiO_2 films deposited at different temperatures.

TiO_2 are observed in the XRD patterns, indicating the formation of a small among of rutile TiO_2 in the films. As it was reported that rutile TiO_2 is the stablest and densest structure of TiO_2 with a mass density of 4.25 g/cm^3, while the anatase TiO_2 is a metastable and less dense structure, with a smaller density of 3.894 g/cm^3 [43]. The increasing tendency of the refractive index from 2.07 to 2.97 in Figure 1, which can be interpreted by the structure change in the films with increasing the growth temperature, is probably due to the film densification with the change from amorphous to anatase as well as the formation of rutile phase [44].

The change of defects in the TiO_2 films was characterized by measuring the room-temperature PL spectra at different growth temperatures. As it was shown in Figure 3, no PL emission was detected from the amorphous TiO_2 films grown below 175°C. A green PL band at around 500 nm was observed from the TiO_2 films with anatase phase grown at temperatures from 200°C to 300°C. In order to study the correlation between the PL and the structure change in the films, the dependences of PL peak intensity and the intensity of (101) anatase peak from the XRD patterns on the growth temperature are plotted together in Figure 4. The PL intensity increases with increasing substrate temperature, reaches a maximum at 250°C, and then decreases strongly at higher growth temperature, which is similar to the growth temperature dependence of the (101) anatase peak intensity in the XRD patterns. This similarity indicates that the defects related to the green PL band are probably located on the (101) oriented surface of the anatase TiO_2 crystals. Finally, the strong quenching of the PL intensity at growth temperature over 250°C is probably due to the degradation of the anatase crystallinity by CVD, which causes an increase of the non-radiative recombination centers in the films.

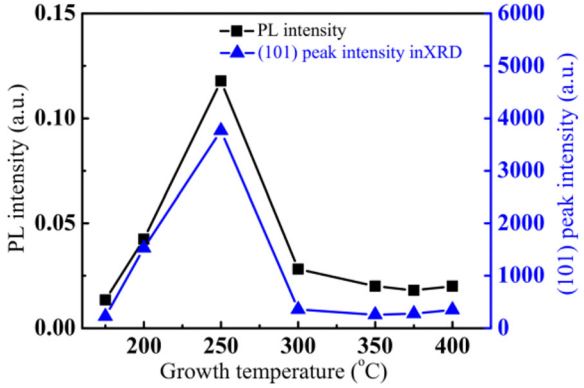

Figure 4 Dependences of the PL intensity and the anatase (101) peak intensity in XRD patterns on the growth temperature.

The thermal stability of the structures in ALD TiO_2 films was studied by annealing two as-grown samples with different initial structures in N_2 atmosphere; one is an amorphous TiO_2 film grown at low substrate temperature of 165°C, and the other is an anatase TiO_2 film grown at 250°C. Figure 5 shows the XRD patterns from the TiO_2 films after annealing the as-grown amorphous sample at different temperatures in N_2 atmosphere for 1 h. Initially, the films are still amorphous at lower annealing temperature below 250°C, then they crystallize to anatase TiO_2 in a very wide annealing temperature range from 300°C to 1,100°C, as shown in the emergence of the (101), (004), and (200) peaks of anatase TiO_2 in the XRD patterns in Figure 5.

Thermal stability of the defects in the annealed TiO_2 films in Figure 5 was characterized by the PL spectra in Figure 6. The PL spectra can be decomposed into a red

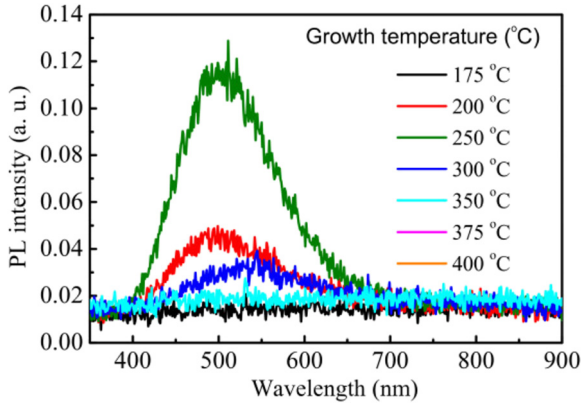

Figure 3 Room-temperature PL spectra from TiO_2 films grown at different temperatures. The spectra were taken under excitation of a 266 nm laser.

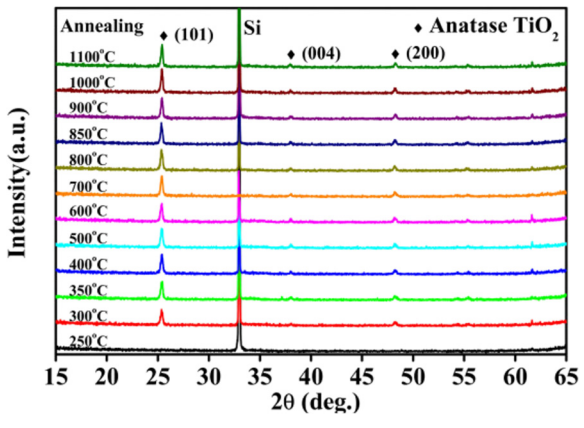

Figure 5 XRD patterns of the TiO_2 films annealed at different temperatures in N_2 atmosphere. The as-grown TiO_2 film is amorphous deposited at a substrate temperature of 165°C.

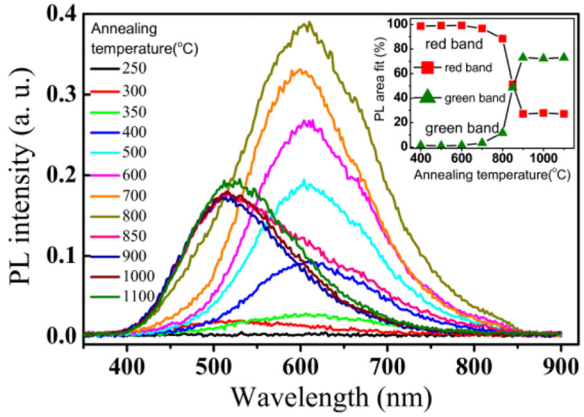

Figure 6 Room-temperature PL spectra of the TiO_2 films annealed at different temperatures in N_2 atmosphere. The as-grown TiO_2 film is amorphous deposited at a substrate temperature of 165°C. The insert is the areal percentages of the red emission band at 600 nm and the green emission band at 515 nm, which are derived from multiple-peak Gaussian fitting of the PL spectra, respectively.

band at 600 nm and a green band at 515 nm. The insert shows the areal percentages of the red emission and the green band, which are derived from multiple-peak Gaussian fitting of the PL spectra, respectively. In conjunction with the XRD patterns in Figure 5, no PL emission is observed from the amorphous TiO_2 films at annealing temperature lower than 250°C. The red PL band was observed from the defects in the anatase TiO_2 films, which were obtained by annealing the as-grown amorphous films at annealing temperatures from 300°C to 800°C. The intensity of the red band increases to a maximum for annealing temperature from 300 to 800°C, and then, it decreases strongly with increasing temperature. For annealing temperature from 800°C to 900°C, the green band appears with the decrease of the red band and the PL spectra undergo a crossover from the red band-dominated emission to the green band-dominated emission as shown in the insert. At even higher annealing temperatures from 900°C to 1,100°C, the PL spectra are dominated by the green band with a saturated intensity.

Figure 7 is the XRD patterns from the TiO_2 films after annealing at different temperatures in N_2 atmosphere for 1 h, in which the as-grown TiO_2 film was initially in anatase phase deposited at a substrate temperature of 250°C. Initially, the annealed TiO_2 films still keep anatase phase in a wide annealing temperature range from 400°C to 900°C, and then, a clear transition from anatase to rutile phase was observed in the annealing temperature range from 950°C to 1,000°C. Finally, the anatase films change to rutile TiO_2 phase at elevated annealing temperatures above 1,000°C.

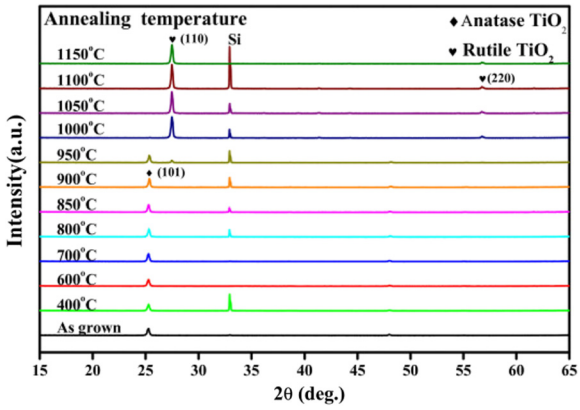

Figure 7 XRD patterns of TiO_2 films after annealing at different temperatures in N_2 atmosphere. The as-grown TiO_2 film is anatase deposited at a substrate temperature of 250°C.

Figure 8 shows the room-temperature PL spectra for the TiO_2 samples in Figure 7 annealed at different temperatures, in which the as-grown film is in anatase TiO_2 phase. The broadband PL emission from the anatase TiO_2 films can be divided into two components with the red peak centered at 600 nm and the green peak centered at 515 nm. Gaussian fitting of the PL spectra was performed using the parameters of the red and green peaks derived from Figure 6. The insert shows the areal percentage of the red and the green components, respectively. The PL spectrum from the as-grown anatase TiO_2 film contains 24% of the red component and 76% of the green component. With increasing annealing

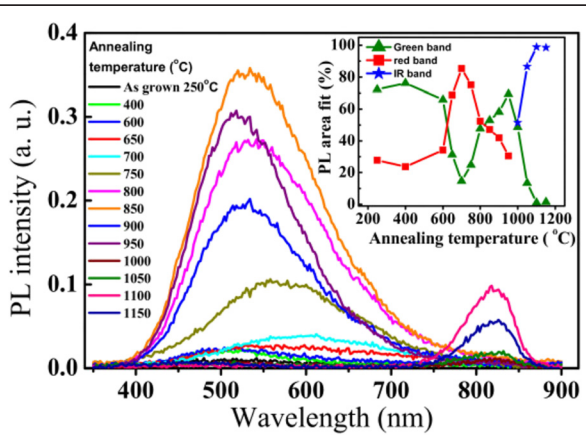

Figure 8 Room-temperature PL spectra of the TiO_2 films annealed at different temperatures in N_2 atmosphere. The as-grown TiO_2 film is anatase deposited at a substrate temperature of 250°C. The insert is the areal percentages of the red emission band at 615 nm, the green emission band at 510 nm, and the near-infrared peak at 820 nm, which are derived from multiple-peak Gaussian fitting of the PL spectra, respectively.

temperature from 400°C to 700°C, the PL intensity of the sample increases slightly, the red component of the spectra increases from 24% to 85%, while the green component reduces from 76% to 15%; therefore, the PL spectra exhibit a red shift. For increasing the annealing temperature from 700°C to 850°C, a strong increase of the PL intensity was observed, the red component decreases from 85% to 47%, while the green component rises from 15% to 53% in the spectra, the relative increase of the green component causes a blue shift of the PL peak. Further increasing the annealing temperature from 850°C to 1,000°C, the PL peaks in the visible spectral range decrease dramatically due to the transition from the anatase to rutile TiO_2 phase. Finally, the PL spectra show a near-infrared peak at 820 nm from the defects in rutile TiO_2 formed at elevated annealing temperatures above 1,000°C.

XPS spectroscopy was studied after annealing the as-grown amorphous TiO_2 films at different temperatures. Figure 9 shows the XPS peaks of Ti $2p_{3/2}$ and Ti $2p_{1/2}$ from the TiO_2 film annealed at 1,000°C after removing 3-nm surface layer by Ar^+ ion sputtering (a), the film annealed at 1,000°C without Ar^+ ion sputtering (b), and the film annealed at 800°C without Ar^+ ion sputtering (c). The binding energies of Ti $2p_{3/2}$ and Ti $2p_{1/2}$ peaks of Ti^{4+} ions in the sample annealed at 1,000°C are located at about 458.75 and 464.48 eV, respectively. After the removal of 3-nm surface layer by Ar^+ ion sputtering, the Ti $2p_{3/2}$ peak shifts to lower energy at 458.54 eV and a shoulder peak at a lower energy of 457.0 eV appears. Multiple-peak Gaussian fitting of the spectrum indicates that the peak at lower energy belongs to the valence state of Ti^{3+} ions in the TiO_2 film, which are formed by Ar^+ ion sputtering, as reported in ref. [32,45,46]. The presence of the Ti^{3+} states in the films causes a small shift of the $2p_{3/2}$ peak of Ti^{4+} ions to lower energy compared to the un-sputtered one in Figure 9b. As a consequence, comparing the $2p_{3/2}$ peak of Ti^{4+} in the sample annealed at 800°C (c) with the one annealed at 1,000°C (b), a slight shift of Ti $2p_{3/2}$ peak from 458.75 to lower energy of 458.46 eV was also observed for the sample annealed at 800°C (c). This suggests that a small amount of trivalent Ti^{3+} ions exist in the sample annealed at 800°C. The relative concentration of the Ti^{3+} ions with respect to the total Ti atoms in the annealed anatase TiO_2 films can be calculated from the integrated intensity of the $2p_{3/2}$ peak of Ti^{3+} ions (red dashed peak), which was derived by multiple-peak Gaussian fitting of the Ti $2p_{3/2}$ peak of the XPS, as shown by the dashed curves in Figure 9.

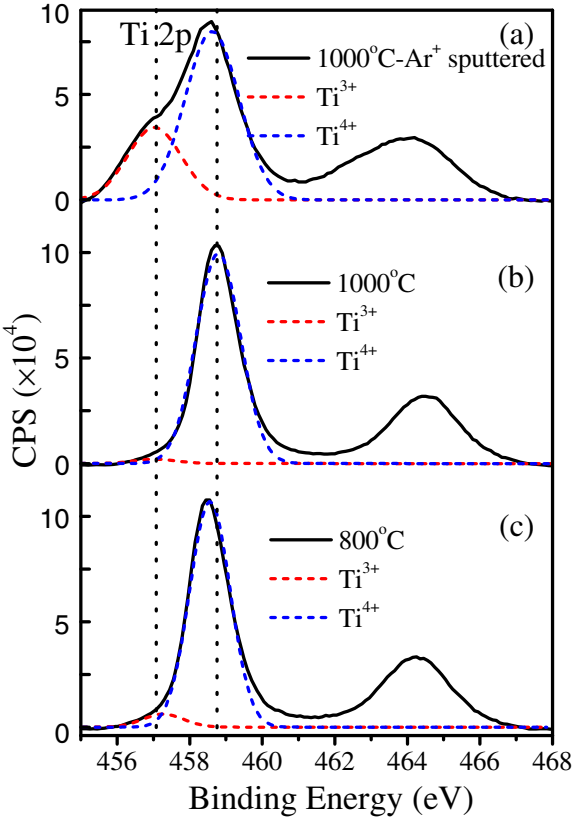

Figure 9 XPS spectra of Ti 2p states from the TiO_2 films. Samples were annealed at 1,000°C after removing 3-nm surface layer by Ar^+ ion sputtering **(a)**; annealed at 1,000°C without Ar^+ ion sputtering **(b)**; and annealed at 800°C without Ar^+ ion sputtering **(c)**. The dashed curves are multiple-peak Gaussian fitting of the Ti $2p_{3/2}$ peak with two components from the valence states of Ti^{4+} (blue) and Ti^{3+} (red).

In order to clarify the correlation between the photoluminescence and the defects related to the under-coordinated Ti^{3+} ions in the annealed TiO_2 films, the integrated PL intensity of the red and green peaks as well as the percentage of Ti^{3+} in the films are plotted together as functions of the annealing temperature in Figure 10, in which the integrated PL intensity of the red and green peaks is derived by multiple-peak Gaussian fitting of the PL spectra in Figure 6. The integrated intensity of the green band was low at annealing temperature below 700°C, it increases from 700°C to 900°C, and then saturated at annealing temperature above 900°C. No obvious correlation was observed between the PL intensity of the green band and the Ti^{3+} ion concentration. The dependence of the integrated PL intensity of the red band on the annealing temperature shows a thermal behavior quite similar to the change of the Ti^{3+} ion concentration. Both of them increased with increasing annealing temperature from 300°C to 800°C, after reaches a maximum at 800°C and then decreases dramatically at annealing temperature varied from 800°C to 900°C. This similarity suggests that the red band may have a strong correlation with the defects associated with the under-coordinated Ti^{3+} ions in anatase TiO_2.

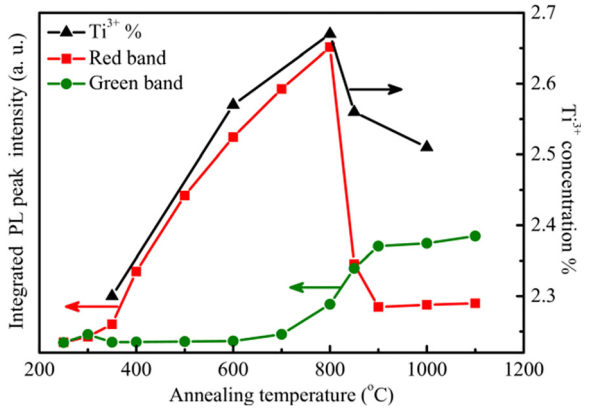

Figure 10 Calculated concentration of Ti^{3+} and the integrated PL intensity. The calculated concentration of Ti^{3+} from XPS analysis (black triangles) and the integrated PL intensity from the red (red squares) and green (green dots) bands is derived from the Gaussian fitting of the XPS and PL spectra of the TiO_2 films after annealing at different temperatures. The solid lines are for a guide of eyes.

Olson et al. [47] calculated the energies for creation of various defects, such as oxygen vacancy and Ti^{4+} and Ti^{3+} interstitials in TiO_2. The formation energy is 24.10 eV (E_1) for oxygen vacancy, which is higher than that for Ti^{3+} interstitial ($E_2 = -40.5$ eV) and Ti^{4+} interstitial ($E_3 = -77.23$ eV). The negative values of E_2 and E_3 indicate that the formation of the defects of under-coordinated Ti^{3+} is energetically favorable. Therefore, defects of Ti^{4+} interstitials and under-coordinated Ti^{3+} may form in higher priority at low annealing temperature during the crystallization of anatase crystal TiO_2 from the as-grown amorphous film. Thus, the red band associated with electron traps of under-coordinated Ti^{3+} dominates the PL spectra at low annealing temperature in Figure 6. The defects of under-coordinated Ti^{3+} can be created with the removal of oxygen atoms by annealing in an inert N_2 atmosphere or by Ar^+ ion sputtering. The removal of oxygen atom can create lone pair electrons to two neighboring Ti^{4+}, and then, electrons will reduce Ti^{4+} to Ti^{3+}. This is confirmed by our XPS study in Figure 9.

Concerning the green PL band from the anatase TiO_2 films, it dominates the PL spectra from the anatase TiO_2 films grown at 250°C or the anatase TiO_2 films which have undergone an annealing process at a high temperature above 850°C. This suggests that origin of the green band is probably from the relative stable surface oxygen vacancies on anatase TiO_2 films. The strong correlation of the green band PL intensity with the intensity of (101) peak in XRD patterns of ALD grown TiO_2 films in Figure 4 reveals that the green PL peak is related to the defects located on (101) surface in the anatase phase. Shi et al. and Mercado et al. [48,49] studied the PL emission from TiO_2 nanocrystals, and they also draw the same conclusion that the green band emission is related to oxygen vacancies on exposed (101) surfaces of anatase TiO_2 nanocrystals. Since the Ti^{3+} ions are unstable, as shown by the dependence of the Ti^{3+} ion density on the annealing temperature in Figure 10, the defects of under-coordinated Ti^{3+} ions can be annealed out, immigrate, and transform into stable surface oxygen vacancies on the anatase TiO_2 films at high annealing temperature from 800°C to 900°C. Figure 6 shows a transition from the red band-dominated PL to the green band-dominated emission with increasing the annealing temperature from 800°C to 900°C. This reveals that some of the under-coordinated Ti^{3+} ions can transform into stable surface oxygen vacancies at high annealing temperature. This causes an increase of the intensity of the green PL band at annealing temperature from 800°C to 900°C. Since only the stable surface oxygen vacancies are preserved at elevated temperature [50]. Finally, the PL spectra are dominated by the green band with a saturation intensity at annealing temperatures above 900°C, as it is shown in Figures 6 and 10. This is also in accordance with the conclusion in ref. [51] that the green-emitting defects are oxygen vacancies located on the surface of anatase TiO_2 films.

From the results of this study and the comprehensive study of the luminescent defects in TiO_2 nanocrystals in ref. [48-51], the proposed model for PL in the ALD TiO_2 films is illustrated in Figure 11. After electrons are excited from the valence band to the conduction band of TiO_2, some electrons are captured by the electron traps associated with under-coordinated Ti atoms, which located at 0.7 to 1.6 eV below the conduction band edge. Radiative recombination of the electrons trapped around under-coordinated Ti atoms with the holes in the valence band contributes to the red band at around 600 to 620 nm. In addition, the green band at around 500 to 520 nm may be from the radiative recombination of free electrons with holes trapped around surface oxygen

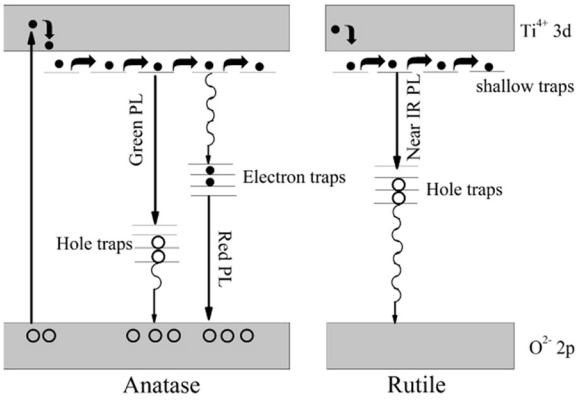

Figure 11 Models for photoluminescence from the electronic transitions of trap states in anatase and rutile TiO_2.

vacancies, which were located at 0.7 to 1.4 eV above the valence band edge. In addition, the near-infrared emission band at around 820 nm is from the defects in rutile TiO_2, which are related to the radiative recombination of electrons in conduction band with hole traps on the (110) and (110) facets of oxygen vacancies [49].

Conclusions

TiO_2 films were grown on silicon substrates by ALD using TDMAT precursor and ozone. A wide ALD growth window was observed between 100°C and 250°C with a self-limiting saturated growth rate of 0.46 Å/cycle. The film is amorphous at the growth temperatures of 165°C and then exhibits anatase crystal phase at the growth temperatures of 250°C. The initial amorphous TiO_2 sample crystallizes to anatase phase with annealing temperature from 300°C up to 1,100°C, while the initial anatase TiO_2 film transfers to rutile phase at elevated annealing temperature above 950°C. Photoluminescence spectra from the defects in the anatase TiO_2 films contain a red band at 600 nm and a green band at 515 nm. XPS and XRD studies indicate that the red band has a strong correlation with the defects of under-coordinated Ti^{3+} ions and the green band is related to the oxygen vacancies located on the (101) surface of the anatase TiO_2 films. The blue shift of the photoluminescence reveals that the defects in anatase TiO_2 film undergo a transition from under-coordinated Ti atoms to surface oxygen vacancies with increasing annealing temperature from 800°C to 900°C in N_2 atmosphere.

Abbreviations

ALD: atomic layer deposition; PL: photoluminescence; TDMAT: tetrakis-(dimethylamino) titanium; XRD: X-ray diffraction; XPS: X-ray photoelectron spectroscopy; RCA: Radio Corporation of America; CVD: chemical vapor deposition.

Competing interests

The authors declare that they have no competing interests.

Authors' contributions

CYJ performed the data analysis and drafted the manuscript. BL performed the growth of the samples, taking the analysis of XRD patterns and PL spectra. ZXL perform the technical support of the PL and XPS analysis. JMS carried out the design and the preparation of the study, supervised the work, and critically read the manuscript. All authors read and approved the final manuscript.

Acknowledgements

One of the authors would like to acknowledge Mrs. C.M. Shi for assisting in X-ray diffraction analysis. This work was supported by the Chinese "973" project (no. 2013CB632102) and National Natural Science Foundation of China NSFC (nos. 61275056 and 60977036).

Author details

[1]Key Laboratory of Weak Light Nonlinear Photonics, Ministry of Education, School of Physics, Nankai University, Weijin Road 94, Tianjin 300071, China. [2]Air Force Aviation University, Nanhu Road No. 2222, Changchun 130022, China.

Received: 17 November 2014 Accepted: 27 January 2015
Published online: 28 February 2015

References

1. Tang H, Prasad K, Sanjinès R, Schmid PE, Lévy F. Electrical and optical properties of TiO_2 anatase thin films. J Appl Phys. 1994;75:2042.
2. Chao S, Wang WH, Lee CC. Low-loss dielectric mirror with ion-beam-sputtered TiO_2-SiO_2 mixed films. Appl Opt. 2001;40:2117–82.
3. Yokogawa T, Yoshii S, Tsujimura A, Sasai Y, Merz J. Electrically pumped CdZnSe/ZnSe blue-green vertical-cavity surface-emitting lasers. J J Appl Phys, Part 2: Letters. 1995;34:L751–3.
4. Fukuda H, Namioka S, Miura M, Ishikawa Y, Yoshino M, Nomura S. Structural and electrical properties of crystalline TiO_2 thin films formed by metalorganic decomposition. J J Appl Phy. 1999;38:6034.
5. Stephen AC, Wang XC, Hsieh MT, Kim HS, Gladfelter WL, Yan JH. MOSFET transistors fabricated with high permittivity TiO_2 dielectrics. IEEE Trans Electron Devices. 1997;44:104–9.
6. Fujishima A, Honda K. Photolysis-decomposition of water at the surface of an irradiated semiconductor. Nature. 1972;238:37–8.
7. O'Regan B, Gratzel M. A low-cost, high-efficiency solar cell based on dye-sensitized colloidal TiO_2 films. Nature. 1991;353:737–40.
8. Mills A, Davies RH, Worsley D. Water purification by semiconductor photocatalysis. Chem Soc Rev. 1993;22:417–25.
9. Maness PC, Smolinski S, Blake DM, Huang Z, Wolfrum EJ, Jacoby WA. Bactericidal activity of photocatalytic TiO_2 reaction: toward an understanding of its killing mechanism. Appl Environ Microbiol. 1999;65:4094–8.
10. Paz Y, Luo Z, Rabenberg L, Heller A. Photooxidative self-cleaning transparent titanium dioxide films on glass. Mater Res Soc. 1995;10:11.
11. Poulios I, Spathis P, Grigoriadou A, Delidou K, Tsoumparis P. Protection of marbles against corrosion and microbial corrosion with TiO_2 coatings. J Environ Sci Health Part A. 1999;34:1455–71.
12. Cai R, Hashimoto K, Itoh K, Kubota Y, Fujishima A. Photokilling of malignant cells with ultrafine TiO_2 powder. Chem Soc Japan. 1991;64:4.
13. Lazar MA, Varghese S, Nair SS. Photocatalytic water treatment by titanium dioxide: recent updates. Catalysts. 2012;2:572–601.
14. Sakai H, Baba R, Hashimoto K, Kubota Y, Fujishima A. Selective killing of a single cancerous T24 cell with TiO_2 semiconducting microelectrode under irradiation. Chem Lett. 1995;24:185–6.
15. Dutta PK, Ginwalla A, Hogg B, Patton BR, Chwieroth B, Liang Z, et al. Interaction of carbon monoxide with anatase surfaces at high temperatures: optimization of a carbon monoxide sensor. J Phys Chem B. 1999;103:4412–22.
16. Xu Y, Yao K, Zhou X, Cao Q. Platinum-titania oxygen sensors and their sensing mechanisms. Sens Actuators B. 1993;14:492–4.
17. Phillips LG, Barbano DM. The influence of fat substitutes based on protein and titanium dioxide on the sensory properties of lowfat milks. J Dairy Sci. 1997;80:2726–31.
18. Tryk DA, Fujishima A, Honda K. Recent topics in photoelectrochemistry: achievements and future prospects. Electrochim Acta. 2000;45:2363–76.
19. Montereali RM. Point defects in thin insulating films of lithium fluoride for optical microsystems. In: Nalwa HS, editor. Handbook of thin film materials volume 3 ferroelectric and dielectric thin films. San Diego San Francisco New York Boston London Sydney Tokyo: Academic Press; 2002. p. 399–431.
20. Leskela M, Ritala M. Atomic layer deposition (ALD): from precursors to thin film structures. Thin Solid Films. 2002;409:138–46.
21. Sneh O, Clark-Phelps RB, Londergan AR, Winkler J, Seidel TE. Thin film atomic layer deposition equipment for semiconductor processing. Thin Solid Films. 2002;402:248–61.
22. Ritala M, Leskelä M, Nykänen E, Soininen P, Niinistö L. Growth of titanium dioxide thin films by atomic layer epitaxy. Thin Solid Films. 1993;225:288–95.
23. Ritala M, Leskelä M, Johansson L-S, Niinistö L. Atomic force microscopy study of titanium dioxide thin films grown by atomic layer epitaxy. Thin Solid Films. 1993;228:32–5.
24. Aarika J, Aidla A, Sammelselgb V, Siimon H, Uustare T. Control of thin film structure by reactant pressure in atomic layer deposition of TiO_2. J Cryst Growth. 1996;169:496–502.
25. Aarik J, Aidla A, Uustare T, Sammelselg V. Morphology and structure of TiO_2 thin films grown by atomic layer deposition. J Cryst Growth. 1995;148:268–75.
26. Aarik J, Aidla A, Kiisler AA, Uustare T, Sammelselg V. Effect of crystal structure on optical properties of TiO_2 films grown by atomic layer deposition. Thin Solid Films. 1997;305:270–3.
27. Kumagai H, Matsumoto M, Toyoda K, Obara M, Suzuki M. Fabrication of titanium oxide thin films by controlled growth with sequential surface chemical reactions. Thin Solid Films. 1995;263:47–53.

28. Kukli K, Ritala M, Schuisky M, Leskelä M, Sajavaara T, Keinonen J, et al. Atomic layer deposition of titanium oxide from TiI_4 and H_2O_2. Chem Vap Deposition. 2000;6:303–10.
29. Schuisky M, Aarik J, Kukli K, Aidla A, Hårsta A. Atomic layer deposition of thin films using O_2 as oxygen source. Langmuir. 2001;17:5508–12.
30. Aarik J, Aidla A, Uustare T, Kukli K, Sammelselg V, Ritala M, et al. Atomic layer deposition of TiO_2 thin films from TiI_4 and H_2O. Appl Surf Sci. 2002;193:277–86.
31. Lim GT, Kim D-H. Characteristics of TiOx films prepared by chemical vapor deposition using tetrakis-dimethyl-amido-titanium and water. Thin Solid Films. 2006;498:254–8.
32. Xie Q, Jiang YL, Detavernier C, Deduytsche D, Van Meirhaeghe RL, Ru GP, et al. Atomic layer deposition of TiO_2 from tetrakis-dimethyl-amido titanium or Ti isopropoxide precursors and H_2O. J Appl Phys. 2007;102:083521.
33. Dennis M, Hausmann EK, Becker J, Gordon RG. Atomic layer deposition of hafnium and zirconium oxides using metal amide precursors. Chem Mater. 2002;14:4350–8.
34. Cleveland ER, Henn-Lecordier L, Rubloff GW. Role of surface intermediates in enhanced, uniform growth rates of TiO_2 atomic layer deposition thin films using titanium tetraisopropoxide and ozone. J Vac Sci Technol A. 2012;30:01A150.
35. Kurtz RL, Stock-Bauer R, Msdey TE, Román E, De Segovia J. Synchrotron radiation studies of H_2O adsorption on TiO_2(110). Surf Sci. 1989;218:178–200.
36. Katamreddy R, Omarjee V, Feist B, Dussarrat C. Ti source precursors for atomic layer deposition of TiO_2, STO and BST. ECS Trans. 2008;16:113–22.
37. Kim YW, Kim DH. Atomic layer deposition of TiO_2 from tetrakis-dimethylamido-titanium and ozone. Korean J Chem Eng. 2012;29:969–73.
38. Rai VR, Agarwal S. Surface reaction mechanisms during plasma-assisted atomic layer deposition of titanium dioxide. Phys Chem C. 2009;113:12962–5.
39. Nam T, Kim JM, Kim MK, Kim H, Kim WH. Low-temperature atomic layer deposition of TiO_2, Al_2O_3, and ZnO thin films. J Korean Phy Soc. 2011;59:452–7.
40. Xie Q, Musschoot J, Deduytsche D, Van Meirhaeghe RL, Detavernier C, Van den Berghe S, et al. Growth kinetics and crystallization behavior of TiO_2 films prepared by plasma enhanced atomic layer deposition. J Electrochem Soc. 2008;155:H688.
41. Elam JW, Schuisky M, Ferguson JD, George SM. Surface chemistry and film growth during TiN atomic layer deposition using TDMAT and NH3. Thin Solid Films. 2003;436:145–56.
42. Norton ET, Amato-Wierda Jr C. Kinetic and mechanistic studies of the thermal decomposition of $Ti(N(CH_3)_2)_4$ during chemical vapor deposition by in situ molecular beam mass spectrometry. Chem Mater. 2001;13:4655–60.
43. Tang H, Lévy F, Berger H, Schmid P. Urbach tail of anatase TiO_2. Phys Rev B. 1995;52:7771–4.
44. Mathews NR, Morales ER, Cortés-Jacome MA, Toledo Antonio JA. TiO_2 thin films - Influence of annealing temperature on structural, optical and photocatalytic properties. Sol Energy. 2009;83:1499–508.
45. Gouttebaron R, Cornelissen D, Snyders R, Dauchot JP, Wautelet M, Hecq M. XPS study of TiOx thin films prepared by d.c. magnetron sputtering in Ar-O2 gas mixtures. Surf. Interface Anal. 2000;30:527–30.
46. Hashimoto S, Tanaka A. Alteration of Ti 2p XPS spectrum for titanium oxide by low-energy Ar ion bombardment. Surf Interface Anal. 2002;34:262–5.
47. Olson CL, Nelson J, Islam MS. Defect chemistry, surface structures, and lithium insertion in anatase TiO_2. J Phys Chem B. 2006;110:9995–10001.
48. Shi JY, Chen J, Feng ZC, Chen T, Lian YX, Wang XL, et al. Photoluminescence characteristics of TiO_2 and their relationship to the photoassisted reaction of water/methanol mixture. J Phys Chem C. 2007;111:693–9.
49. Mercado CC, Knorr FJ, McHale JL, Usmani SM, Ichimura AS, Saraf LV. Location of hole and electron traps on nanocrystalline anatase TiO_2. J Phys Chem C. 2012;116:10796–804.
50. McHale JL, Rich CC, Knorr FJ. Trap state photoluminescence of nanocrystalline and bulk TiO_2: implications for carrier transport. MRS Proc. 2010;1268:EE03–8.
51. Diebold U. The surface science of titanium dioxide. Surf Sci Rep. 2003;48:53–229.